

RESEARCH ARTICLE

New nuclear magic numbers

Reiner Krücken*

*Physik Department E12, Technische Universität München, Garching, Germany**(May 2010)*

The nuclear shell model is a benchmark for the description of the structure of atomic nuclei. The magic numbers associated with closed shells have long been assumed to be valid across the whole nuclear chart. Investigations in recent years of nuclei far away from nuclear stability at facilities for radioactive ion beams have revealed that the magic numbers may change locally in those exotic nuclei leading to the disappearance of classic shell gaps and the appearance of new magic numbers. These changes in shell structure also have important implications for the synthesis of heavy elements in stars and stellar explosions. In this review a brief overview of the basics of the nuclear shell model will be given together with a summary of recent theoretical and experimental activities investigating these changes in the nuclear shell structure.

Keywords: Nuclear shell model, magic numbers, nuclear structure, exotic nuclei, radioactive beam facilities, nuclear spectroscopy, nuclear reactions

1 Introduction

The atomic nucleus, core of the atom, is the carrier of essentially all visible mass in the Universe. Atomic nuclei are also the fuel for the burning of all stars and are thus the source of the energy enabling life on this planet. Nuclear reactions are also at the heart of the production of all naturally occurring chemical elements from deuterium to uranium.

Despite this central role of atomic nuclei and nuclear reactions in the Universe, the structure and dynamics of atomic nuclei cannot yet be satisfactorily described on the basis of the fundamental underlying theory of the strong interaction, quantum chromodynamics (QCD). This results from the fact that the protons and neutrons inside the atomic nucleus are themselves complex systems built up from quarks and gluons, the force carriers of the strong interaction. Thus the strong interaction between nucleons is an effective, van der Waals like interaction that governs a two-component quantum many-body system, making analytical calculations impossible. The free nucleon-nucleon interaction can be measured via scattering experiments and is well described theoretically. However, inside an atomic nucleus the interaction between two nucleons changes due to the presence of the other nucleons or, in other words, the nuclear matter in which the nucleons are submerged. Therefore, effective interactions have to be used to describe the interaction of protons and neutrons inside an atomic nucleus. Much progress has been made in recent years to derive effective interactions that are motivated by the symmetry properties of QCD but which also take into account the effects of the nuclear medium on the nucleon-nucleon interaction [1, 2, 3, 4]. It is one of the central goals of modern nuclear physics to develop a unified theoretical framework that allows one to reliably predict the properties of complex nuclei with a set of theoretical tools, which are based on the same underlying basic ingredients connected to the QCD symmetry properties.

*Email: reiner.kruecken@ph.tum.de

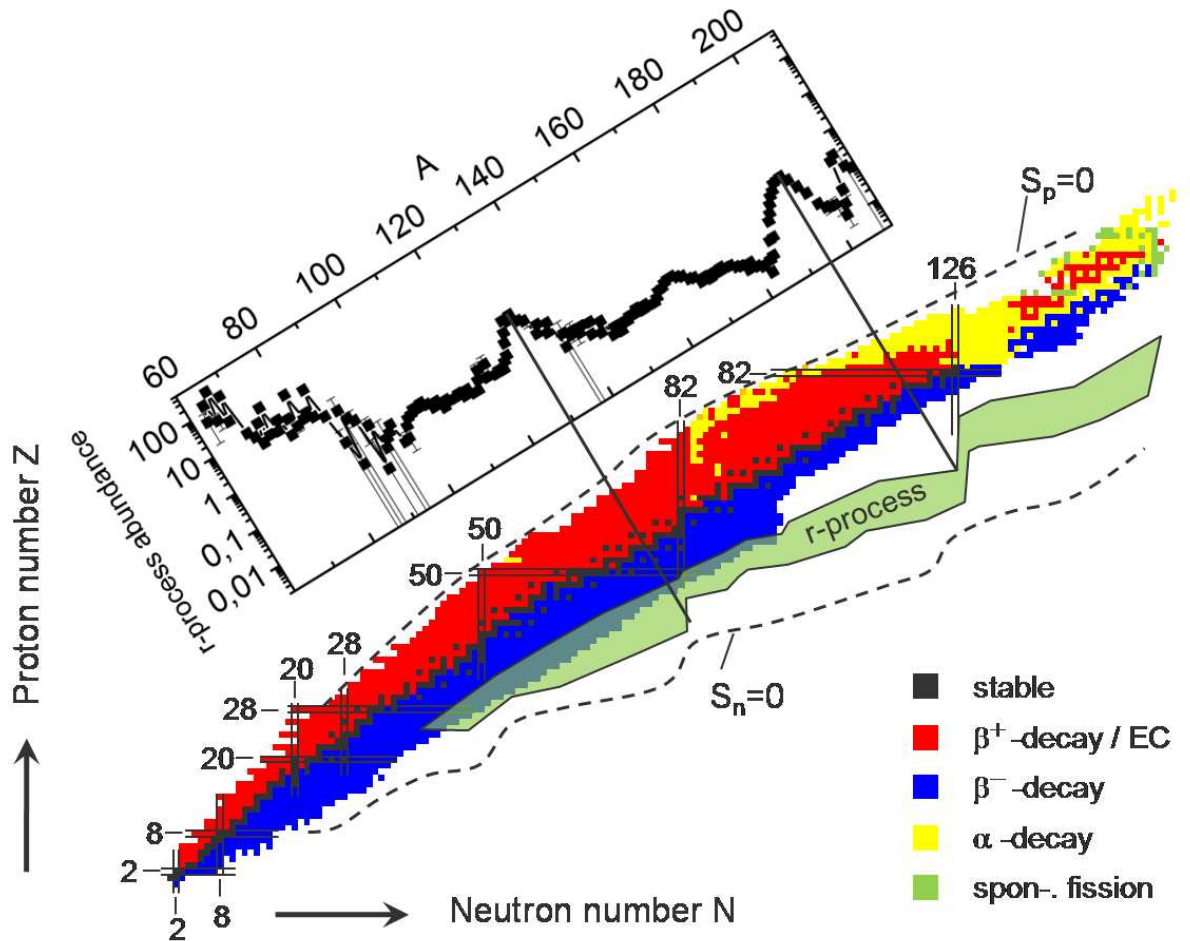


Figure 1. Nuclear chart with indicated classic shell closures and r-process path. The dashed lines indicate roughly where we believe that nuclei are bound or in other words that the neutron and proton separation energies S_n , S_p are positive. Also shown are solar r-process abundances, taken from [17].

In the recent decades nuclear structure physics has undergone a major re-orientation and rejuvenation seeing the discovery of new phenomena and the emergence of new frontiers. In particular the availability of energetic beams of short-lived (radioactive) nuclei, in the following also referred to as rare isotope or exotic nuclear beams, has opened the way for the exploration of the structure and dynamics of complex nuclei in regions far away from stability, where very limited information is available. These new experimental capabilities allow one to delineate the limits of nuclear existence and study the dependence of the nuclear force on proton and neutron number (or isospin¹). They also enable us to study the behavior of nuclei near and beyond the neutron and proton drip-lines and to investigate the emergence of new modes of nuclear behavior, not observed near stability. The neutron (proton) drip-line denotes the line beyond which the separation energy S_n (S_p) for the last neutron (proton) becomes negative and thus no additional neutron (proton) can be bound by the nuclear force². Examples for such new modes are nuclear halos, skins of protons or neutrons, and new modes of excitation were protons and neutrons decouple as well as new isospin pairing phases and new decay modes [7, 8, 9, 10, 11, 12, 13, 14].

¹Proton and neutron are treated as two different projections $T_z = -1/2$ and $T_z = +1/2$, respectively, of an isospin $T = 1$ state.

²Note that a proton with $S_p < 0$ can be bound to the nucleus by the Coulomb barrier. Such nuclei can decay by proton radioactivity, the tunneling of the proton through the Coulomb barrier [6].

One of the major successes in the description of the properties of atomic nuclei is the introduction of the nuclear shell model. The shell structure was observed (see e.g. [15, 16]) in the occurrence of special numbers of protons and neutrons in nuclei, so called magic numbers, for which discontinuities appear, e.g. in binding energies and separation energies (the energies needed to remove the last neutron or proton). Also other experimental observables, such as energies of first excited states in even-even nuclei, and electromagnetic transition rates show these shell effects. By analogy to the very successful atomic shell model these magic numbers were taken as evidence of closed shell configurations in atomic nuclei, similar to the noble gas configurations in the electron shells of atoms. The classical magic numbers are indicated as horizontal and vertical lines in the nuclear chart shown in Fig. 1.

Until recently the persistence of these magic numbers throughout the whole nuclear chart was a fundamental paradigm in nuclear physics. However, in the last two decades sophisticated experiments with exotic nuclear beams made it possible to scrutinize the persistence of the shell gaps far away from stability. The measurements showed some surprising changes in the nuclear shell structure as a function of proton and neutron number in light nuclei. These observations triggered numerous theoretical investigations, which in turn made new predictions that some magic numbers will disappear and new shell gaps will appear in certain regions of the nuclear chart.

The shell structure in nuclei plays also an important role in defining the pathways on the nuclear chart of various processes of the synthesis of the chemical elements in the Universe (see [18] for a recent review) and results in specific features of the observed solar abundances [19].

In particular, the possibility of a quenching of shell gaps in neutron-rich medium mass and heavy nuclei has been discussed in the context of reproducing the r-process abundances [20, 21, 22] in network calculations. The rapid neutron capture (r-)process is responsible for the production of about half of the heavy elements above iron. It proceeds in a very neutron-rich, high entropy environment where certain seed nuclei capture neutrons until an equilibrium abundance of isotopes for an element (Z) is reached between neutron capture and photo-dissociation in the hot environment [23]. Beta-decay out of this equilibrium distribution leads to the next heavier element ($Z+1$) where again neutron capture occurs until an equilibrium abundance distribution is reached and beta decay leads to the next heavier element. By this mechanism all heavy elements above iron can be produced. The most abundant isotope in an isotopic chain under equilibrium conditions can be estimated for a given neutron flux by a characteristic value of the neutron separation energy S_n [18] with the equation

$$S_n(\text{MeV}) = \frac{T_9}{5.04} \left(34.075 - \log n_n + \frac{3}{2} \log T_9 \right),$$

where T_9 is the temperature in units of 10^9 K and n_n is the neutron density in cm^{-3} . This equation implies that the r-process proceeds along a path of constant neutron separation energies, which is indicated in Fig. 1. Once the neutron density drops sufficiently the process falls out of equilibrium. After the neutron capture stops for lack of neutrons the neutron-rich nuclei decay via beta decay towards stability to produce the observed r-process abundances.

The shell structure along the r-process path is imprinted in the abundance pattern, since the beta-decay half-lives drop significantly just after the shell closure and thus abundance is collected along the neutron-shell closure. The broad abundance peaks in the r-process abundances at masses $A=130$ and $A=195$ (see Fig. 1) are a result of this. If, for example, the shell closures at $N=82$ and $N=126$ persist in neutron-rich nuclei, the r-process path will flow along these shell closures at these mass numbers. However, if the shell gaps are quenched or if shell gaps occur for different neutron (or proton) numbers, the path of constant separation energies may be shifted and the r-process path may be located further away or closer to stability.

Thus, the underlying nuclear physics of nuclei far off stability can have a significant impact on pathways of nucleosynthesis. Certainly the astrophysical conditions at the nucleosynthesis

sites will be decisive for the element production. In case of the r-process the astrophysical site has not yet been clearly identified. One of the favorite scenarios is the neutrino-driven wind in core-collapse supernovae of massive stars [24, 25, 26]. However, neutron-star mergers are also being considered as a possible site [27]. It will take the combined effort of multidimensional astrophysical modeling, precision astronomical observations of elemental and isotopic abundances as well as precise knowledge of the nuclear physics of exotic nuclei to solve the puzzle of the origin of the heavy elements.

In this article I will try to provide a brief review of the recent developments concerning the modification of shell structure far away from stability. I will start by recapitulating some of the basic features of the nuclear shell model and by introducing the main ingredients for shell model calculations. On the basis of these foundations I will try to summarize how shell structure may change as one goes away from stability. After that I will provide some overview of how one may look experimentally for shell closures and provide examples of recent experiments that have helped to discover the disappearance of classic shells and the appearance of new magic numbers.

2 Basics of the nuclear shell model

The underlying concept for the nuclear shell model is the idea that nucleons move almost independently inside a central potential well. However, contrary to atomic physics, where the central potential for the electrons originates from the charge of the atomic nucleus, the central potential for a nucleon is the result of its interactions with the other nucleons in the atomic nucleus.

2.1 Independent particle model

The concept of independent particle motion seems surprising if one looks at the well known radial dependence of the nucleon-nucleon potential (see fig. 2) with its short range repulsion (at about 0.5 fm) and its strongly attractive component, which can be described by pion exchange. Aside from this central part the nucleon-nucleon interaction also contains spin-orbit, spin-spin, and tensor components¹. As a result of the strong short range repulsion the nucleons have a large kinetic energy at short distances and the total energy, as sum of potential and kinetic energy, shows only a relatively weak binding at distances of 1.5-2 fm. This saturation property of the nuclear force also leads to the almost constant density of the nuclear matter inside nuclei. The resulting central potential can be approximately described by an inverted Fermi-function, the so-called Woods-Saxon potential (WS) (see Fig. 3) or alternatively by a harmonic oscillator (HO) potential with an additional term proportional to the square of the orbital angular momentum, in order to effectively flatten the potential in the nuclear interior.

As a result of the central potential one obtains groups of energy levels forming shells separated by large energy gaps as indicated in Fig. 3. By filling these individual shells consistent with the requirements of the Pauli exclusion principle one obtains closed inert configurations, similar to the noble gas configurations in atoms, for certain numbers of protons and neutrons, the so called magic numbers (2, 8, 20, 28, 50, 82, 126). The first attempts to explain the observed magic numbers with a nuclear shell model failed until in 1949 Mayer, Haxel, Suess and Jensen [29, 30] showed that the inclusion of a strong spin-orbit interaction with a sign opposite to that known from the fine structure in atoms gave rise to the observed gaps between the nuclear shells. The original form of this spherical mean field was:

$$U(r) = \frac{1}{2}m\omega^2r^2 + D\vec{\ell}^2 + C\vec{\ell} \cdot \vec{s}. \quad (1)$$

¹ The tensor interaction will play an important role later on in this review.

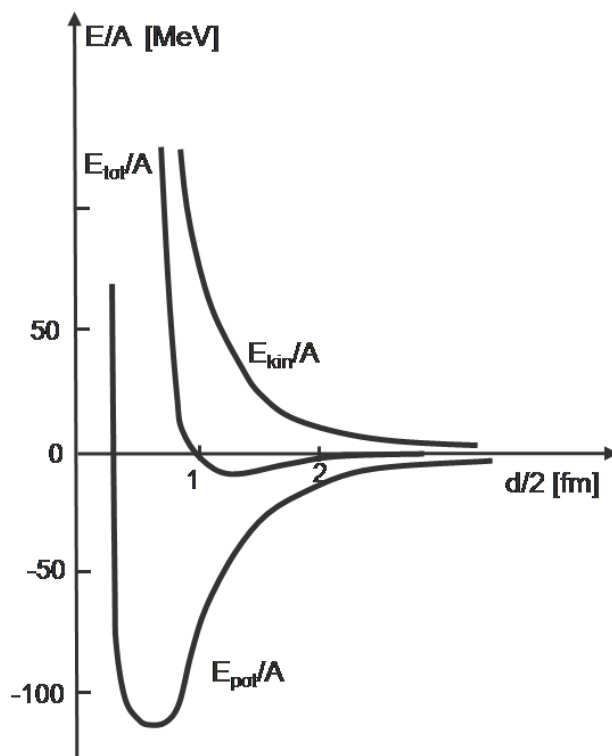


Figure 2. Potential and kinetic part of the radial part of the nucleon-nucleon interaction resulting in a total energy with a weak binding at distances of 1.5-2 fm (Adopted from [28]).

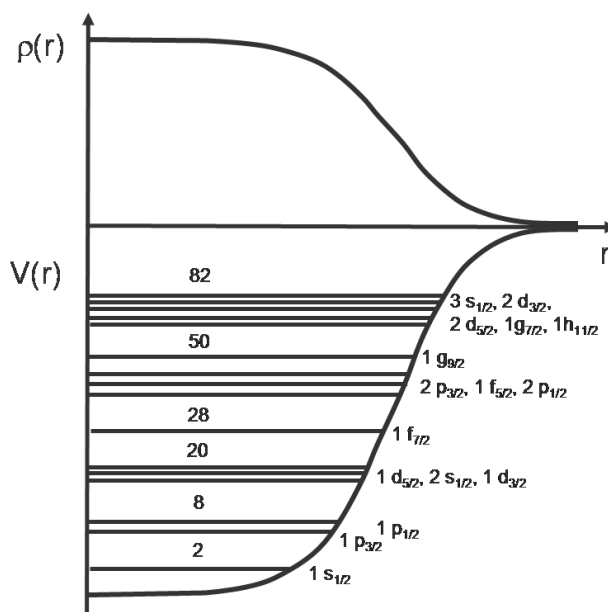


Figure 3. Woods-Saxon type mean field with clustering of single-particle levels into major shells. In the top of the figure the corresponding radial density distribution is indicated.

The exact ordering within the shells depends on the choice of potential, HO vs. WS, and their parameters. Please note also that there is a mass dependence in these parameters, most obvious due to the change of the radius of the potential well proportional to $A^{1/3}$. Today a more realistic mean field potential can be self-consistently calculated using Hartee-Fock methods based on effective nucleon-nucleon interactions [31, 32].

Already with the concept of independent particles moving in this potential, a one-body mean field potential, a broad body of experimental data can be explained, in particular for nuclei with only one particle or hole outside a magic core, e.g. ground state spins, excited states, magnetic moments. However, this model certainly is too naive since the potential well cannot account for all aspects of the interaction between the nucleons. This leads to so-called core-polarization effects where the particles outside the magic core will have some influence on the core itself, which can have dramatic effects, e.g. on magnetic moments. In addition one has to take into account a residual interaction among the nucleons outside the magic core. This residual interaction plays a major role in the excitation spectrum of nuclei away from the magic shells and will be discussed in the following subsection.

2.2 Interacting shell model

In a realistic shell model calculation the residual interaction has to be taken into account between all valence particles outside an appropriately chosen closed core of fully occupied shells. For this appropriate choice one has to ensure that excitations from this closed configuration do not play a role in the excitation spectrum of the nucleus. In order to perform an interacting shell model calculation one defines a configuration space of single-particle orbits for the valence nucleons, which can interact. The configuration space is limited in size by taking into account only a limited number of orbits outside the chosen closed core and also ignoring higher lying unoccupied levels not relevant for the properties of the nuclei of interest (see Fig. 4).

The single-particle energies (SPE) for the calculations may be taken from a modern self-consistent mean-field calculation or from experimental single-particle energies. The residual interaction between the valence particles is taken into account by means of two-body matrix elements (TBME) $\langle j_1, j_2, J | V | j_3, j_4, J \rangle$ for all possible combinations of orbitals j_i in the model space¹, where J is the total angular momentum to which the two single-particles angular momenta couple. An effective interaction V for a specific model space has to include all possible combinations of orbitals j_i and generally depends on spin and isospin. From the SPEs and TBMEs the excitation spectra of all nuclei for a given configuration space can be calculated. For example, in the sd shell, involving the $1s_{1/2}$, $1d_{3/2}$, and $1d_{5/2}$ levels and thus neutron numbers $N=8-20$ and proton numbers $Z=8-20$, the SPE of 3 levels and 63 TBME have to be known [35]. These are then used as input for the determination of the energies and wave-function of about 10^6 nuclear states in the mass region $A = 17 - 39$.

TBMEs can in principle be derived from the bare nucleon-nucleon interaction, which has been measured in nucleon-nucleon scattering, using the so-called G-matrix theory [36, 37]. However, in order to account for changes of the nucleon-nucleon interaction in the nuclear medium some adjustments, e.g. incorporating short-range repulsion and core polarization, have to be included. In addition the extracted effective interaction has typically to be modified empirically to fit to existing data (see Refs. [5, 38, 39, 40, 41] for extensive reviews).

2.3 Monopole shift of the single-particle energies

A central interaction $V(|\vec{r}_1 - \vec{r}_2|)$ that depends only on the distance $|\vec{r}_1 - \vec{r}_2|$ between the two particles can be expanded within a complete set of functions, e.g. Legendre polynomials $P_k(\cos \theta_{12})$:

$$V(|\vec{r}_1 - \vec{r}_2|) = \sum_k \nu_k(r_1, r_2) P_k(\cos \theta_{12}), \quad (2)$$

¹In principle also three-body interactions have to be taken into account and their influence is a topic of current investigations [33, 34].

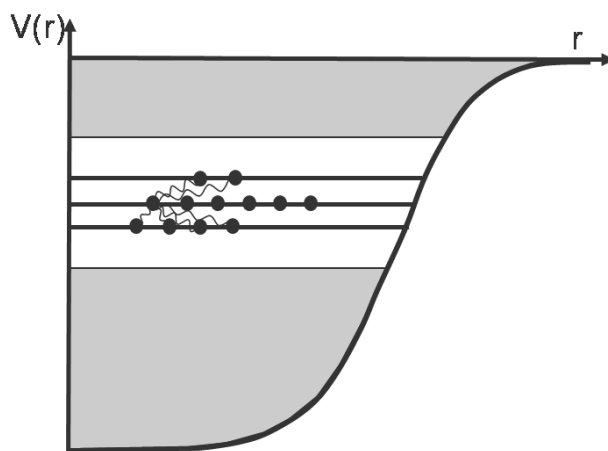


Figure 4. Basic ingredient for an interacting SM calculation. Single-particle energies (SPE) in the configuration space and two-body-matrix elements (TBME) of the interaction between the nucleons in the configuration space. A closed shell core and unoccupied orbits above the configuration space are not part of the SM diagonalization and are colored in grey.

with coefficients $\nu_k(r_1, r_2)$ and $\theta_{12} = \langle \vec{r}_1, \vec{r}_2 \rangle$. The most important multipole orders relevant for the shell structure in nuclei are the monopole component and the quadrupole component. The latter plays an important role in driving the system to quadrupole deformed shapes, which will be discussed later on.

The average of the interaction over all directions

$$V_{j_i, j'_k} = \frac{\sum_J (2J + 1) \langle j_i, j'_k, J | V | j_i, j'_k, J \rangle}{\sum_J (2J + 1)} \quad (3)$$

is equal to the monopole component of the interaction between two nucleons (i, k denote if they are proton π or neutron ν) in orbitals with angular momenta j and j' , respectively, and is of particular importance for the discussion of changing shell structure since it has a direct influence on the energy spacing of the single-particle levels.

The effect of the monopole component can be seen best when looking at the so-called effective single-particle energies (ESPE) [46, 47]. For a specific level the ESPE is defined as the separation energy of this orbit calculated with the bare SPE of the configuration space and including the effects of the monopole interaction with all other levels in the configuration space. Thus the spacing between the ESPEs defines the energies for the excitation of individual nucleons, and thus the effective shell gaps. It should be pointed out here that the monopole interaction is not the only relevant aspect of the residual interaction. However, its influence on the ESPE as a function of proton or neutron number is one of the most decisive contributions with respect to changing shell gaps.

It was recently pointed out by Otsuka and collaborators [48, 49, 50, 51] that various changes in the shell structure are caused by the monopole effect of the tensor force, an important component in the free nucleon-nucleon interaction which had not been considered explicitly before in shell-model calculations. The tensor force is one component of the residual interaction and results from the ρ and π meson exchange term of the nucleon-nucleon interaction. The important realization was that in particular the monopole effect of the tensor force between protons and neutrons depends on whether the orbits of these valence nucleons are $j_> = \ell + s$ or $j_< = \ell - s$. The effect of this interaction component is that if protons and neutrons are in $j_<$ and $j_>$ or vice versa the single particle energies are lowered (more bound), while in case that both are in $j_<$ or both are in $j_>$ orbits the single particle energies are raised (less bound), as indicated in Fig. 5. Otsuka and collaborators also showed that the evolution of shell structure in exotic nuclei could be described by a so called monopole-based universal interaction V_{MU} [51], consisting of a Gaussian central force, containing many complicated processes including multiple meson exchanges, and a tensor

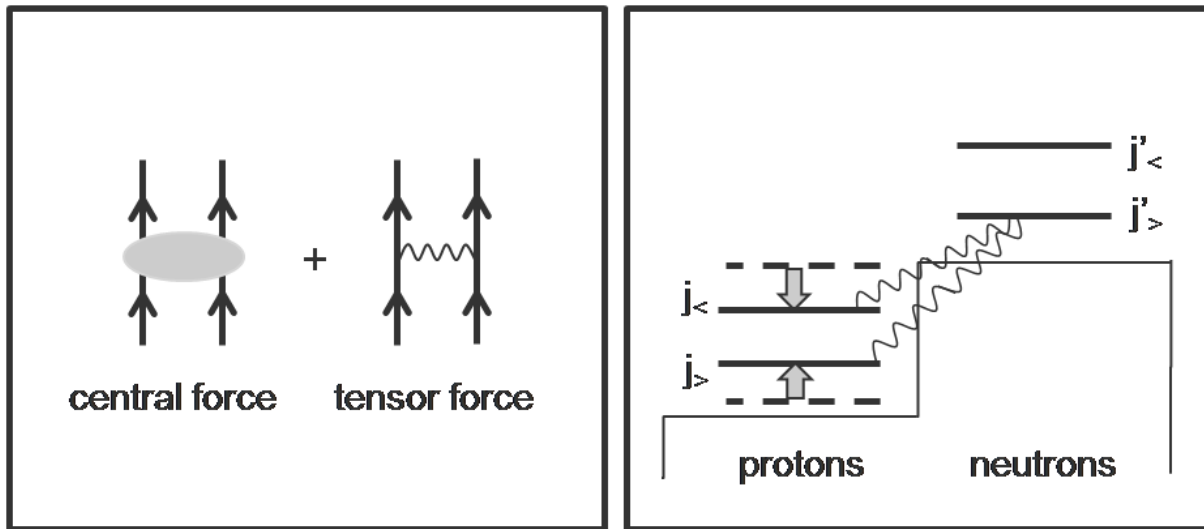


Figure 5. *Left*: Basic components of the monopole interaction, a Gaussian central force and a tensor force. (adopted from [51]). *Right*: Schematic effect of the monopole interaction between a $j'_>$ neutron orbital and $j'_<$ and $j'_>$ proton orbits.

force comprised of ρ and π meson exchange, as schematically indicated in the left of Fig. 5.

The effect of the tensor force can be seen in Fig. 6 where the effective single particle energies for neutrons are shown for the $N=51$ isotones as a function of proton number Z . The figure shows how the EPSEs for the neutron $\nu 3s_{1/2}$, $\nu 2d_{3/2}$, $\nu 1g_{7/2}$, and $\nu 1h_{11/2}$ levels change relative to the $\nu 2d_{5/2}$ level as protons are added to the $\nu 1g_{9/2}$ orbital. The dashed lines show the effect of the monopole part of a Gaussian central force only, while the solid lines include the effect of the monopole part of the tensor force. One can see the dramatic effect on the $j'_<$ neutron $\nu 1g_{7/2}$ orbital as its $j'_>$ spin partner proton $\nu 1g_{9/2}$ orbital is filled between $Z=40$ and 50. At the same time the energy of the $j'_>$ neutron $\nu 1h_{11/2}$ orbital is raised by the repulsive effect of the tensor force. The effect of the tensor force is particularly strong between spin-partner orbits due to the fact that the radial wave-functions are the same and thus the short range interaction can have maximum effect.

I will discuss the role of this interaction in the evolution of shell structure and the occurrence of new magic numbers in section 4.

3 Experimental probes of magic numbers

In this section I want to briefly review some of the experimental methods that enable us to explore the evolution of shell structure and magic numbers in exotic nuclei. One may ask, why not simply measure the single-particle energies. However, as will be discussed below, such experiments are quite challenging and it is often easier to resort to other data, which are more readily available, such as measuring nuclear masses or investigating the excitation energies and collectivity in even-even nuclei. However, first of all it is necessary to briefly explain how exotic nuclei are produced and made available for experiments.

3.1 Production of exotic nuclear beams

In the production of exotic nuclear beams one generally distinguishes between two methods.

The first method, called Isotope Separation On Line (ISOL) method employs light ion beams that induce spallation, fission, or fragmentation reactions in a primary target, from which the short-lived reaction products only escape by diffusion. They are then singly ionized using e.g. surface ionization or element specific laser ionization techniques. The ions are extracted from the

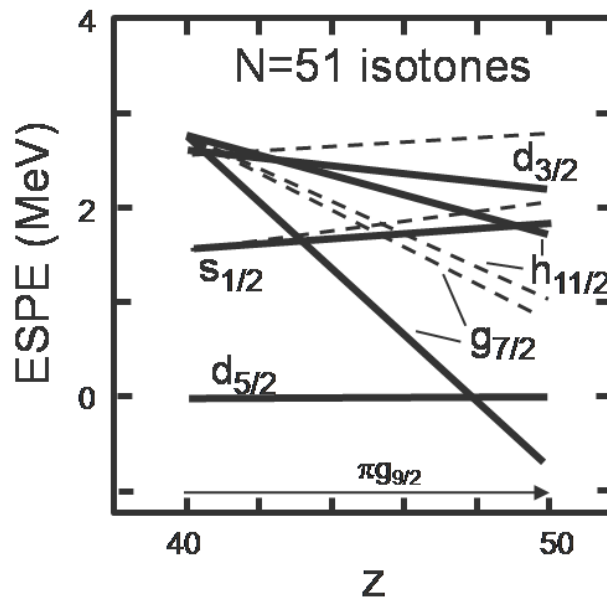


Figure 6. Evolution of the neutron effective single particle energies (ESPE) for the N=51 isotones as the proton $\pi g_{9/2}$ level is filled (adopted from [51]). The dashed lines are for the central force only, while the solid lines include both the central force and the tensor force.

primary target and can be delivered to low-energy experiments, such as a beta-decay station, a laser-spectroscopy set-up, or a Penning Trap for mass-measurements. Alternatively, they can be injected into a secondary post-accelerator for acceleration to energies of around 2-10 MeV per nucleon, which are energies on the scale of the Coulomb barrier between the nuclei. These Coulomb-energy beams are used for inelastic scattering experiments or nucleon transfer reactions, which are discussed below. Since the diffusion out of the production target depends on the chemical properties, ISOL facilities cannot provide secondary beams of all elements. Also, the diffusion takes some time, limiting the reach of the ISOL methods to exotic nuclei with half-lives of at least some 10 ms. The most important ISOL facilities worldwide are REX-ISOLDE at CERN, HRIBF at ORNL and ATLAS at ANL in the U.S.A., ISAC at TRIUMF in Canada, and SPIRAL at GANIL in France.

The second method relies on the production of exotic nuclei by the fragmentation or fission of a high-energy (50-1000 MeV per nucleon) heavy ion beam in a production target, from which the reaction products emerge with beam velocity. The nuclei of interest are separated and identified by means of a large acceptance magnetic fragment separator. The separated nuclei are used for secondary reaction experiments at intermediate and relativistic energies (40-1000 MeV per nucleon) or can be stopped for decay studies. They can also be injected into a storage ring for mass-measurements. Since the separation technique does not depend on chemical properties all elements are accessible in in-flight experiments. Also nuclei with half-lives as low as a few hundred ns can be used for experiments since the nuclei move at a large percentage (40-80%) of the speed of light. Current world-leading in-flight facilities are the NSCL at MSU in the U.S.A., GSI Darmstadt in Germany, GANIL in France, and RIBF at RIKEN in Japan. With the FAIR Project at GSI Darmstadt with a planned begin of operations around 2017/18 the reach of the current facility towards more exotic nuclei will be significantly extended.

NSCL and FRIB, with a planned startup around 2017, at MSU in the U.S.A. plan to combine the in-flight production and separation with a gas-stopping cell from which ions can be extracted and fed into a post-accelerator for secondary experiments at Coulomb-barrier energies.

3.2 *Masses, binding energies, separation energies*

One of the first indications for the occurrence of a shell gap can come from the mass of the nucleus, which can today be measured even for nuclei with production rates of a few per second and half-lives in the millisecond range.

The most precise technique to measure masses employs Penning Traps and can achieve an accuracy of 10 keV and better [52, 53]. As do all high precision measurements today, these experiments rely on a frequency measurement. The ions with charge q and mass m are stored in a Penning trap by the superposition of a strong homogeneous magnetic field B for radial confinement and a weak static electric field for axial trapping. The electric field is applied to hyperbolic electrodes with axial symmetry around the B-field direction. The electrode is fourfold segmented and the ions are excited by a radio-frequency applied to the pairs of segments. In case the applied radio-frequency is equal to the cyclotron frequency $\omega_c = B \cdot q/m$, maximum energy is transferred to the ion. When the ion is extracted from the trap its time-of-flight to a detector is measured. Measuring the time-of-flight as a function of the applied radio-frequency reveals a resonance pattern with a minimum time-of-flight for the cyclotron frequency of the ion, from which the mass can be extracted.

In an alternative approach masses of nuclei can be measured in a storage ring [54, 55] in which they circulate with about 10^6 revolutions per second, with the revolution frequency depending on q/m of the ion. In order to suppress effects on the revolution frequency resulting from the velocity spread of the ions one can perform the experiment in two different ways. One technique relies on the operation of the storage ring in a so called isochronous mode, where the circulation time of the ions does not depend on their velocity [56]. A measurement of the time-of-flight using special detectors allows one to measure the revolution frequency, which now only depends on q/m . The other method relies on cooling of the ions in an electron cooler to reduce their velocity spread to a negligible value. In this case the revolution frequency can be measured by the Schottky noise signal induced by the ions in an electrode installed in the ring, which is then analyzed by applying a Fast Fourier Transformation [57].

The measured masses can be used to investigate the shell evolution due to the fact that nuclei with a closed shell configuration are bound more strongly compared to nuclei with one or a few extra nucleons. Thus one can see indications for a shell closure either by an enhanced binding energy of the nuclei with closed shells or by a significantly reduced separation energy for additional nucleons. For example, the neutron separation energy S_n for a nucleus with Z protons and A nucleons is given by

$$S_n = BE(Z, A) - BE(Z, A - 1) = [M(Z, A - 1) - M(Z, A) + M_n] \cdot c^2.$$

Here $BE(Z, A)$ is the binding energy of a nucleus with mass $M(Z, A)$ and M_n is the neutron mass.

Figure 7 shows neutron separation energies S_n for oxygen, calcium, and lead isotopes as a function of neutron number. One can clearly see the jumps in the separation energies for the well known classic magic numbers $N=126$ in lead, $N=20, 28$ in calcium and $N=8$ in oxygen.

However, local shifts in the binding energies or separation energies can sometimes also be the result of other causes, e.g. the competition and mixing of different nuclear shapes at low energies. Therefore, the ground state properties alone are not always sufficient to establish a new shell gap or the disappearance of a known shell gap. However, important additional information can be gained from the study of excited states.

3.3 *Excited states and collectivity*

Additional evidence for a shell closure can come from low lying excited states in nuclei. For example, in nuclei with one particle or hole outside a closed shell the excited states directly provide information on the single-particle states.

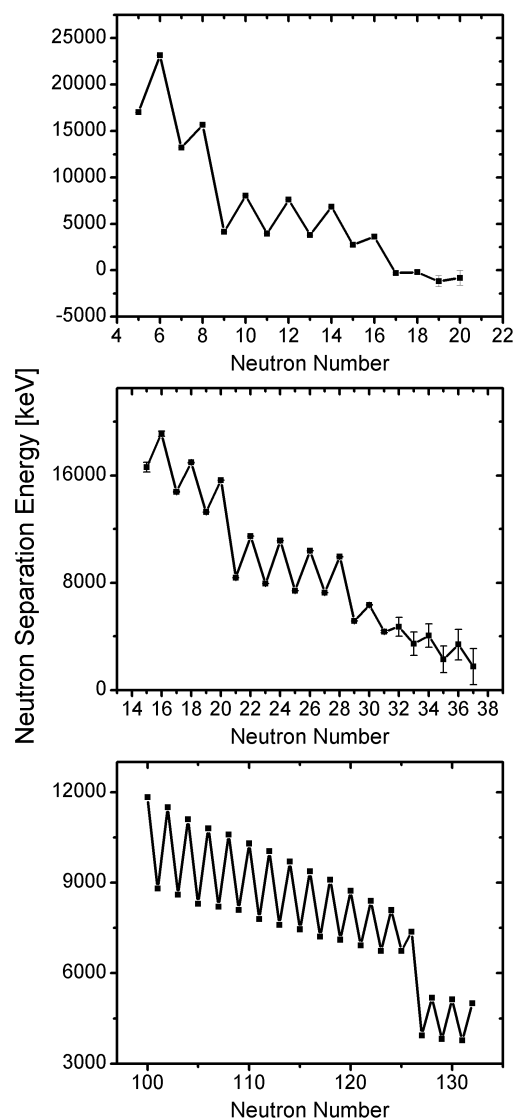


Figure 7. Neutron separation energies S_n for oxygen (top), calcium (middle), and lead (bottom) isotopes taken from [58], respectively.

For exotic nuclei with production rates between about 1 per second and 1 per hour it is possible to study the gamma-decay of excited states populated either in the radioactive decay of the mother nucleus or in the decay of a long-lived isomeric state populated in the production reaction of the exotic nucleus. In either case the subsequent gamma-decay can be observed establishing the sequence of excited states and their electromagnetic decay. However, the total angular momentum and parity of the emitting state can be established only by measuring angular distributions or correlations of the gamma-radiation depopulating this level, which requires significant statistics and thus is often not possible in exotic nuclei. Lacking this information, the observation of states in nuclei with only one particle or hole outside a closed shell is only partially helpful since not all quantum numbers of the relevant states can be established.

However, even-even nuclei, with an even number of protons and neutrons, enable a more simple access to the investigation of shell structure. The well known pairing interaction, that couples the angular momenta of like nucleons pairwise to total angular momentum 0, leads to the lowering of the energy of 0^+ states in even-even nuclei. As a result all even-even nuclei have a spin and parity $J^\pi = 0^+$ ground state and a simple low-energy excitation spectrum with a 2^+ first excited state in almost all cases. Therefore, an explicit measurement of angular momentum and parity

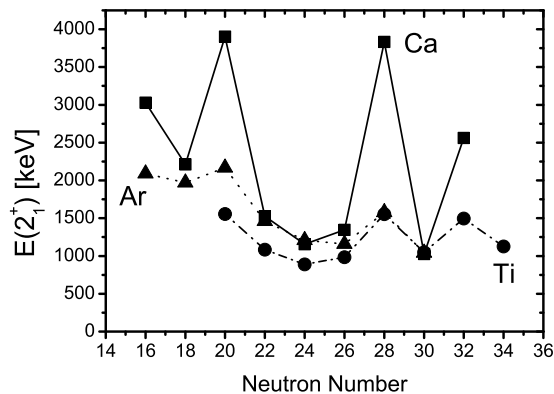


Figure 8. Experimentally known energies of the first excited 2^+ states in the even-even Ar, Ca, and Ti isotopes

of this first excited state in even-even nuclei is basically not needed. At the same time its energy is a good indicator for the existence of a shell closure, as can be understood by the following considerations.

In order to generate an excited 2^+ state in a doubly magic nucleus at least one nucleon has to be excited across the shell gap, since all single-particle levels are fully occupied and coupled to a total spin $J = 0$, such that a simple recoupling of angular momenta to $J = 2$ is not possible. The cross-shell excitation costs a large amount of energy, leading to a high excitation energy of several MeV for the 2^+ state. In even-even nuclei with one closed and one open shell it does cost significantly less energy to produce this excited state, namely the energy to break a pair of nucleons in the open shell, about 1-1.2 MeV.

Fig. 8 shows the energies of the lowest 2^+ states in the even-even Ar, Ca, and Ti isotopes. The high excitation energies at the classic neutron magic numbers 20 and 28 are clearly visible for all three elements, while the highest energies occur in case of the doubly magic nuclei ^{40}Ca and ^{48}Ca . The high excitation energy of the 2^+ state in ^{52}Ca and ^{54}Ti is due to the filling of the $\nu 2p_{3/2}$ orbital, which consists of a sub-shell.

If both shells for protons and neutrons are open it is energetically less costly to produce excited 2^+ states since the long range quadrupole-quadrupole interaction between the valence protons and neutrons allows for surface vibrations (near the closed shells) (≈ 0.6 MeV) and a permanent quadrupole deformation (mid shell) with low lying rotational excitations (≈ 0.05 -0.4 MeV). Rotational and vibrational excitations are so-called collective excitations where several/many nucleons are coherently contributing to the overall motion of the nucleus, in one case surface vibrations of quadrupole shape ¹ and in the other case the rotation of a quadrupole shaped charge distribution. In both cases a large (collective) transition matrix element $\langle 2^+ | \hat{Q} | 0^+ \rangle$ exists for the electromagnetic quadrupole operator $\hat{Q} = r^2 Y_{20}$. The value of this matrix element is orders of magnitude larger than for the case where a single-nucleon is moved by an electric quadrupole interaction from one single-particle level to another one.

Therefore, the strength of the electromagnetic transition between the 0^+ ground state and the first excited 2^+ state in even-even nuclei provides another indication for shell closures. The strength is often measured in terms of the reduced transition strength $B(E2; 0^+ \rightarrow 2^+) \propto |\langle 2^+ | Q | 0^+ \rangle|^2$. Large $B(E2)$ values are found for collective nuclei near mid-shell while very small $B(E2)$ values will be found at shell closures.

Aside from gamma-ray spectroscopy in decay experiments one can gain access to the first excited 2^+ state in even-even nuclei via inelastic scattering either using electromagnetic (Coulomb) excitation or using the strong-interaction. In the Coulomb excitation of an exotic nuclear beam

¹Also octupole shape vibrations are possible but will not be discussed further here.

the projectile is scattered on a stable high- Z nucleus in order to ensure a strong Coulomb interaction or, in other words, the availability of many virtual photons for the excitation. Coulomb excitation is a very well established technique [59, 60] and theoretically under control since the interaction and the reaction kinematics are well known. It has been adopted for the study of exotic nuclei at beam energies below the Coulomb barrier (see e.g. [61, 62, 63]) as well as at energies well above the Coulomb barrier between projectile and target nucleus, often coined intermediate energy or relativistic Coulomb excitation [13, 64, 65]. In either case the scattered projectiles are observed in coincidence with the characteristic gamma-ray transition from the deexcitation of the first excited 2^+ level.

The advantage of the Coulomb excitation method is that, in addition to the observation of the energy of the 2^+ state, the excitation cross-section can be used to obtain information on the electromagnetic transition matrix element connecting ground state and the 2^+ state. However, one needs to ensure that the interaction is of electromagnetic nature only, which is the case if the distance between the scattering partners stays well above the range of the strong interaction. At beam energies significantly below the Coulomb barrier between the scattering partners this is easily achieved for all scattering angles, and thus the technique is sometimes called "safe" Coulomb excitation. Such experiments are performed at various ISOL facilities. For the "safe" Coulomb excitation at energies below the Coulomb barrier one is restricted to thin targets ($\approx \text{mg}/\text{cm}^2$) and thus experiments need beam intensities of $\approx 10^4$ particles per second or above.

For the Coulomb excitation with high beam energies at in-flight facilities the selection of excitation via pure Coulomb interaction is basically achieved by selecting very small scattering angles, which ensures that the reaction products did not approach each other too closely. The relativistic Coulomb excitation has the advantage that thick targets ($\approx \text{g}/\text{cm}^2$) can be used. This allows one to perform experiments with secondary beam intensities of only ≈ 10 particles per second.

Aside from the pure electromagnetic excitation one can alternatively use the inelastic scattering of the exotic projectile on a target containing Hydrogen (protons) or Helium (alpha particles). Since in this case the projectile is dominantly excited by the strong interaction, one can obtain different information on the excited states. The electromagnetic excitation is only sensitive to the proton contribution while inelastic proton scattering, for example, is also sensitive to the neutron contribution of the transition. See Ref. [13] and references therein for further details.

3.4 *Energies and occupations of single-particle levels*

While masses, 2^+ energies, and transition matrix elements provide important insights as to the existence of a shell closure, it is important, if possible, to obtain direct information on the energies, quantum numbers, and occupations of the single-particle levels above and below a shell closure. In order to obtain this information one needs to measure the quantum numbers and energies of the single-particle energies in nuclei with or near closed shells. This can be done by so-called transfer reactions, in which one or few nucleons are transferred between a projectile and target nucleus in a peripheral collision where both nuclei just touch. Such experiments have been performed for more than 40 years at stable beam accelerators using light projectiles, like protons, deuterons, ^3He , or ^4He . For example, a neutron can be placed in the empty single-particle levels outside a closed shell nucleus, e.g. ^{48}Ca , using a deuteron beam and detecting the residual proton from this (d, p) reaction. In this case the neutron can be placed in the $\nu 2p_{3/2}$, $\nu 1f_{5/2}$, or $\nu 2p_{1/2}$ levels in ^{49}Ca . The energies and angular momentum quantum numbers of the populated levels can be measured by detecting energies and angular distributions of the residual protons, e.g. with a high resolution magnetic spectrograph. Such experiments can be performed within a day or so at beam intensities of 10^{10-12} particles per second (pps) and with beam energies of around 10 MeV per nucleon or higher.

For short lived exotic nuclei this technique has to be modified by applying inverse kinematics. At various ISOL facilities, post-accelerated exotic nuclear beams are used to induce (d, p) neutron

transfer reactions in deuterated polyethylene foils to study the neutron single-particle energies far away from stability. In such experiments the protons from the target are detected in silicon detector arrays surrounding the target, measuring energies and emission angles. Due to the energy loss of the heavy-ion beam in the target and due to kinematic effects resulting from the reversed scattering geometry the energy resolution in such experiments is rather poor. However, one can use gamma-ray detection in coincidence with the detected protons to select excited states of interest. Experiments of this kind need beam intensities of at least 10^4 particles per second.

Another way to probe the energies, quantum numbers, and occupations of single-particle levels in a doubly magic nucleus is the so-called knockout reaction [7, 13] with relativistic beams at in-flight facilities. In these experiments a fast secondary exotic nuclear beam is directed onto a thick ($\approx \text{g/cm}^2$) carbon or beryllium target at typical energies of 50-1000 MeV per nucleon. Due to the use of thick targets, which is enabled by the high beam energies, experiments can be performed with secondary beam rates of as low as 1 particle per second. In this case each incoming particle can be identified in its mass and charge through measurements of the magnetic rigidity, time-of-flight (providing velocity), and energy loss, which depends on the nuclear charge Z . In the knockout reaction a nucleon at the surface of the projectile is knocked out of its orbital by a peripheral collision with the target nucleus. The residual nucleus with one less nucleon is again guided through a magnetic spectrometer that on one hand allows for an event-by-event identification of the knockout reaction products¹ and on the other hand yields a precise measurement of the momentum change of the projectile like residue compared to that of non reacted projectiles.

The change in momentum of the residue is, due to momentum conservation, a direct measure of the momentum of the single-particle that was removed from its orbital in each individual reaction. For many knockout reactions on the same single-particle orbital one obtains a momentum distribution of this particular orbital. By means of a Fourier transformation this distribution is related to the spatial distribution of the radial wave-function of the removed nucleon, which varies for different orbital angular momenta L of the involved single-particle level. Thus the measured momentum distribution for an individual level is characteristic for the orbital angular momentum of the single-particle level from which the nucleon is removed. The cross-section for the knock-out reaction can be reliably calculated using Glauber theory [7] and can be used as a measure of the occupation of the orbital, which can be compared with the prediction of shell model calculations.

Thus, direct reactions like transfer and knockout reactions are essential tools to obtain detailed information on the energies of the single-particle levels and on the number of particles occupying these levels.

4 Changes of shell structure far away from stability

After having provided a rough overview on the theoretical basics of the shell model and the most important experimental observables used to probe the occurrence of shell gaps it is now time to turn towards the recent findings of changing shell structure in exotic nuclei. The discovery of such changes were only possible due to the recent developments in providing energetic beams of exotic nuclei and enabling the investigation of nuclei further and further away from stability. Through these studies it has been possible to significantly extend our knowledge of the evolution of nuclear structure with isospin. Hereafter, I only can highlight a few of the recent developments explicitly, while more information can be found in various reviews, e.g. Refs. [8, 13, 71].

On the theoretical side a number of studies over the years have suggested that shell structure may change far away from stability for a number of reasons [66, 67, 68, 69, 70]. Among the

¹Aside from the knockout reaction various other reactions occur.

various mechanisms for shell changes in the mean-field potential the reduction of the spin-orbit interaction with increasing neutron excess has been discussed extensively. From a phenomenological point of view the spin-orbit interaction $V_{LS} \propto dV(r)/dr$ may be expected to decrease for a more diffuse nuclear potential $V(r)$ that may result from the weaker binding of the additional neutrons.

Alternatively, the monopole shifts originating from the residual interaction of the valence nucleons, as discussed in section 2.3, may cause the shell structure to change dependent on the occupied single-particle levels.

In this section I want to highlight a few examples of regions in the nuclear chart where major changes in the shell structure have been observed or are currently debated. The evolution of all major shell closures has been extensively discussed in a recent review [71], to which the reader is referred to.

I will start in the region of light elements between oxygen and calcium, where the shell structure is modified by the residual interaction. Afterwards I will discuss the situation in heavier nuclei, e.g. near ^{132}Sn , where possible evidence for modifications of the shell structure has been discussed and changes of the spin-orbit interaction as well as effects of the residual interaction have been put forward in this context.

4.1 Light nuclei

Fig. 9 shows the neutron-rich side of the nuclear chart between $Z=7$ (nitrogen) and $Z=22$ (titanium) indicating the stable isotopes in black. The unstable nuclei are mostly indicated in yellow, aside for those nuclei where changes in shell structure are indicated by different colors:

- light blue for the new doubly magic nuclei ^{24}O ($N=16$) and ^{54}Ca ($N=34$) (see below).
- orange for the Island of Inversion (see below), where the $N=20$ shell closure has eroded and deformed configurations based on the pf-shell above $N=20$ dominate the ground state configurations of nuclei near $N=20$.
- green for the $N=28$ isotones ^{42}Si and ^{44}S where experimental data strongly indicates that their ground states are deformed and the $N=28$ shell gap disappears (see e.g. [13, 71] and references therein).

Also listed are the years when the most-neutron-rich isotope of each element was discovered. This indicates our current knowledge of the so called neutron drip-line. The evolution with time, in particular in the last 20 years or so is closely related to the aforementioned developments of radioactive beam facilities. The development of theoretical and experimental predictions went hand in hand. While in some cases, e.g. in case of the Island of Inversion the experimental evidence for the breakdown of the $N=20$ gap came first, in other cases, e.g. the prediction of the $N=34$ shell closure, theoretical predictions motivated experimental activities.

One can also see that the neutron drip line follows an almost linear dependence, aside from odd-even effects. The oxygen isotopes represent a major deviation from this smooth trend with ^{24}O ($N=16$) being the last bound oxygen isotope, despite the fact that the simple shell model expectation would tell us that ^{28}O with 20 neutrons in a closed shell should be favored in terms of nuclear binding. One can also see that if one adds only one additional proton suddenly six more neutrons can be bound in the fluorine isotopes where the last bound isotope is ^{31}F .

4.1.1 Experimental evidence for the $N = 16$ magic number

The first evidence for the $N = 16$ magic number in oxygen came from an evaluation of neutron separation energies on the basis of measured masses. From the neutron separation energies of the oxygen isotopes in Fig. 7 it is apparent that the nucleus ^{28}O with $N=20$ is not bound anymore, despite its classic magic neutron number, which should provide additional stability. To the contrary, one can notice a jump in the oxygen separation energies at $N=16$. This surprising observation was taken as the first indication that instead of $N=20$ there may be a new shell

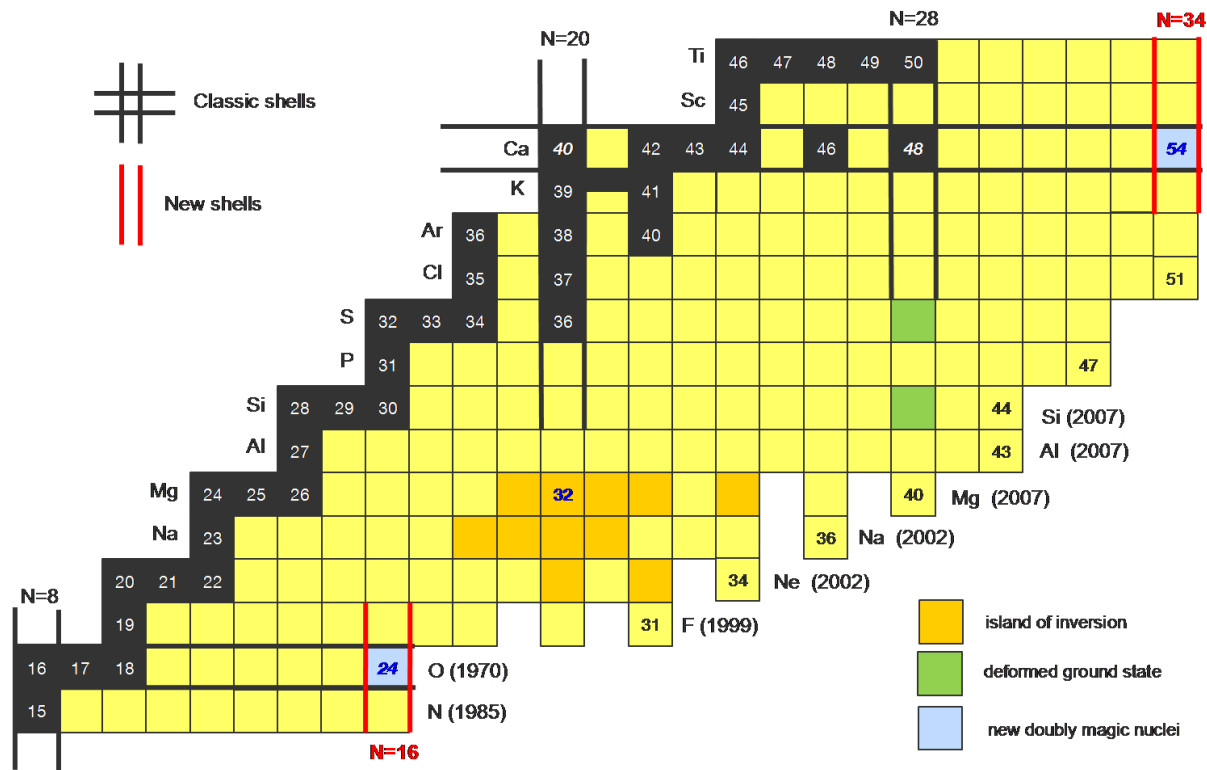


Figure 9. Nuclear chart between nitrogen ($Z=7$) and titanium ($Z=22$) indicating classic and new shell closures as well as the breakdown of classic shell closures.

closure at $N=16$ for oxygen [72].

In a recent experiment at the National Superconducting Cyclotron Laboratory (NSCL) at Michigan State University, USA, the energy of the first excited 2^+ state in ^{24}O could be deduced [73]. Since this state, produced by the removal of a proton and a neutron from an exotic beam of ^{26}F , is unbound, it decays promptly to the ground state of ^{23}O under emission of a neutron. In this experiment ^{26}F nuclei were produced in a first step by fragmenting a ^{48}Ca beam on a Be target and separating and identifying the ^{26}F fragments in the A1900 fragment separator. The ^{26}F fragments were then sent onto a secondary Be target so that ^{24}O was produced by the removal of a proton and a neutron from the ^{26}F beam. By identifying ^{23}O and the decay neutrons at the same time it was possible to reconstruct the energy spectrum of excited states in ^{24}O . The high energy of 4.72 (11) MeV of the 2^+ state provides clear evidence of the spherical nature of ^{24}O , as expected for a doubly magic nucleus.

Further evidence for the doubly magic nature of ^{24}O comes from its single-particle structure, which was studied in a knockout experiment [74] at the Fragmentseparator FRS [75] of the GSI Helmholtzzentrum für Schwerionenforschung in Darmstadt, Germany. In this experiment it was found that the measured momentum distribution for a neutron removal from the ground state in ^{24}O showed a pure $L=0$ character. This proved that the last two neutrons in ^{24}O occupied only the $\nu 2s_{1/2}$ single-particle level as predicted by a shell model calculation including the new shell closure at $N=16$. If there were no new magic number $N=16$ in the oxygen isotopes the $\nu 1d_{3/2}$ level would have been close to the $\nu 2s_{1/2}$ level and a substantial contribution of $L=2$ would have been measured in the momentum distribution, which was not the case.

All experimental evidence available on ^{24}O and its neighboring isotopes clearly support the fact that $N=16$ is a new magic number (see also [13, 71, 76]).

4.1.2 Effective Single Particle Energies for $N=20$

On the basis of the theoretical knowledge concerning the effect of the residual interaction on the single-particle energies the disappearance of the $N=20$ and appearance of the $N=16$ magic

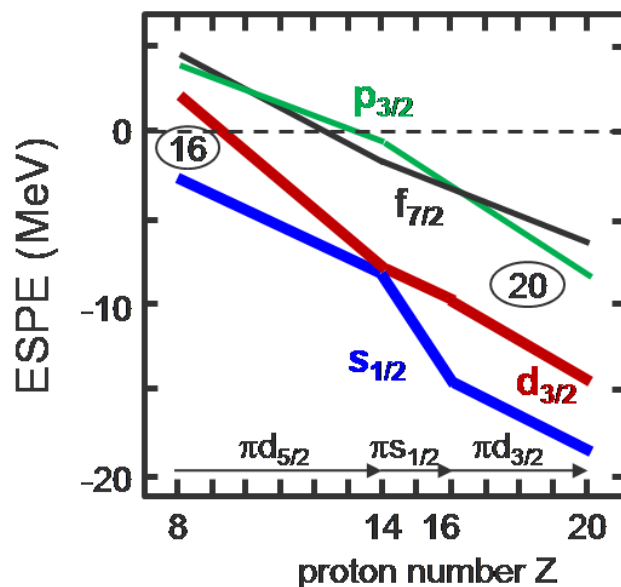


Figure 10. Effective single particle energies (ESPE) for the N=20 isotones between oxygen and calcium (adopted from [51]).

number in the oxygen isotopes can be explained.

Figure 10 shows the effective single-particle energies for the N=20 isotones, adopted from [51], as a result of the monopole component of the residual interaction V_{MU} with Gaussian central and tensor part (see Fig. 5). One can see the large N=20 shell gap for calcium (Z=20), which decreases in size once protons are removed from the $\pi 1d_{5/2}$ orbital below Z=14. At Z=8 a sizable N=16 shell gap is present. The starting point for this plot are the Z=8 SPE from the SDPF-M interaction [47]. Note that ^{28}O is unbound.

By adding protons in the $\pi 1d_{5/2}$ orbital the $\nu 1d_{3/2}$ orbital gets more bound and the classic N=20 shell gap is opening up. The N=16 shell gap for Z=8 is thus due to the absence of the attractive monopole interaction between the $\pi 1d_{5/2}$ the $\nu 1d_{3/2}$ levels.

The effect of the monopole interaction can be also seen when adding a single proton into the $\pi 1d_{5/2}$ orbital. In this case there is some additional binding of the $\nu 1d_{3/2}$ level due to its interaction with the $\pi 1d_{3/2}$ level allowing for the binding of six more neutrons all the way to ^{31}F .

4.1.3 The Island of Inversion

The ESPE for the N=20 isotones in Fig. 10 show another interesting feature for Z=10 and Z=12. For these proton numbers there is no clear shell gap visible. The N=16 shell gap is large only for oxygen and carbon (Z=6) and the N=20 shell gap is well developed only for Z=14 and above. For Ne and Mg there is a more even spacing of all the levels and in this case quadrupole correlations can come into play since their strength is of the order of the level spacing. In such a case quadrupole collectivity can develop by a partial occupation of levels of the pf shell, which in turn drive the ground states of the N=20 isotones ^{30}Ne and ^{32}Mg into deformation. Due to the effective lowering of the pf-shell orbits compared to the standard sd-shell levels, one talks about an inversion of the single-particle levels. The nuclei around ^{30}Ne and ^{32}Mg , which show ground state deformation and thus a breakdown of the N=20 shell, are considered to be part of this so-called *Island of Inversion* [77]. The first proof of the role of deformation for these nuclei came from the Coulomb excitation of an exotic ^{32}Mg beam at the RIPS fragment separator at RIKEN, Japan [64]. However, until today the exact borders of the island of inversion are still not delineated completely and there are still intensive experimental and theoretical efforts underway to exactly understand the evolution of shell structure and the competition of spherical and deformed configurations in this mass region (see e.g. [13, 78, 79, 80] and references therein).

4.1.4 The new magic number $N=34$

When Honma et al. [81] introduced the new effective shell model interaction GXPF1 for the nuclei in the pf-shell, which included the effect of the monopole component of the tensor interaction, they predicted that the first excited 2^+ energy in the $N=34$ nucleus ^{54}Ca would be as high as for the doubly magic $^{40,48}\text{Ca}$ nuclei. At the same time, shell-model calculations using the well established KB3G interaction [77, 82, 83, 84] support a $N = 32$ shell closure, which is experimentally well established, but not a $N = 34$ shell closure.

The prediction of a new doubly magic shell closure for ^{54}Ca triggered a large number of experimental and theoretical investigations. So far, ^{54}Ca has been out of reach and thus the experimental investigations have concentrated on the nuclei in its vicinity. A number of studies have been performed on neutron rich $Z = 20 - 24$ nuclei using β -decay as well as multi-nucleon transfer, Coulomb excitation, and knockout reactions of radioactive ion beams (see [13, 85] and references therein). The level schemes obtained for these nuclei compare favorably with shell-model calculations using the GXPF1A interaction and thus support the prediction of the new $N=34$ shell closure. Clarity concerning this very interesting question will only be obtained when experiments can finally be performed on ^{54}Ca directly. This may be possible within the next few years at the new Radioactive Ion Beam Factory (RIBF) at RIKEN.

4.2 Shell quenching in heavier nuclei

In the preceding chapters one of the main mechanisms for the change of shell structure in neutron-rich nuclei has been discussed, namely the shift of single-particle energies due to the monopole component of the residual interaction. However, self-consistent mean-field studies have also predicted changes in the shell structure, in particular when approaching the neutron-dripline [66, 67, 68, 69, 70]. The most significant effect is the quenching of shell gaps near the dripline due to the coupling of bound states to unbound continuum states above the Fermi-energy, e.g. through pair scattering. In addition, an isospin dependence of the spin-orbit interaction has been discussed. For increasing neutron-to-proton ratios this could lead to a reduction of the splitting between spin-orbit partner orbits, which is the main cause for the shell gaps in medium mass and heavy nuclei. Thus a reduction of the spin-orbit interaction, related to a more diffuse nuclear surface, would also cause a shell quenching.

Experimental evidence for the quenching of the $N=82$ shell was suggested by the observation [86] of a less than expected binding in the $N=82$ nucleus ^{130}Cd , just two neutrons below doubly-magic ^{132}Sn . The binding energy was determined by measuring the beta-decay endpoint energy and thus the mass difference to the daughter nucleus of known mass. The experiment was performed at the ISOLDE radioactive beam facility at CERN, one of the longest operating radioactive beam facilities with a large number of elements available for experiments. However, recent spectroscopic studies of the excited states in ^{130}Cd at GSI Darmstadt revealed that the excitation pattern can be well described by SM calculations in which the $N=82$ shell gap has its full size [87]. The $N=82$ nuclei below ^{130}Cd are just coming into the reach of RIB facilities and the next years will probably solve the puzzle of possible shell quenching below ^{132}Sn .

Another investigation in this mass region studied the evolution of the energy spacing between the proton orbitals $\pi 1g_{7/2}$ and $\pi 1h_{11/2}$ in the antimony (Sb) isotopes as a function of neutron number. An increase of this spacing was observed [88] and is interpreted as a lowering of the $\pi 1g_{7/2}$ and a rise of the $\pi 1h_{11/2}$ orbital, which in turn means that the spacing between the $\pi 1g_{7/2}$ ($\pi 1h_{11/2}$) orbital and its spin-orbit partner orbital $\pi 1g_{9/2}$ ($\pi 1h_{9/2}$) is decreasing with increasing neutron number. This observation was taken as a possible indication of a reduction of the spin-orbit interaction with increasing neutron number. However, Otsuka et al. [49, 50] pointed out that the monopole part of the tensor interaction would produce exactly the same effect, since within the studied range of neutron numbers the $\nu 1g_{9/2}$ orbital is filled. The equivalent effect for neutron orbitals in the $N=51$ isotones has been discussed in section 2.3 and Fig. 6.

In addition to the aforementioned studies, there is also an intense effort to study the persistence

of classic shell closures in exotic nuclei. On the neutron-rich side the $N=50$ shell closure around doubly-magic ^{78}Ni [89, 90, 91, 92] and the $N=126$ below ^{208}Pb [93, 94, 95], which are both relevant for the delineation of the r-process path, have become accessible to first experimental studies. On the proton-rich side the doubly-magic ^{48}Ni has been produced for the first time [96]. ^{48}Ni lies near the proton drip-line and there is evidence that it is unbound against two-proton emission from its ground state [97] where the unbound protons are emitted via tunneling through the Coulomb barrier. See Refs. [6, 12] for recent reviews on decay studies at the proton dripline. Also the heaviest $N=Z$ doubly magic nucleus ^{100}Sn and its immediate vicinity has been reached experimentally and beta decay studies have recently been performed with production rates of about 1 per hour [98, 99, 100, 101].

Another frontier of the investigation of shell closures in nuclei is the question of which shell gaps determine the structure of the superheavy nuclei and if the next spherical shell closure beyond Pb ($Z=82$) is $Z=114$, 120, or 126. Here various theoretical models come to different conclusions [102] and with tremendous experimental efforts it has been possible to expand the nuclear chart up to $Z=118$ using fusion reactions with intense stable ion beams (see Ref. [103, 104] for recent reviews). While apparently there is an increased stability of the heaviest, most neutron-rich superheavy elements observed, the question of the position and size of the next spherical shell closure remains open so far.

5 Conclusion

In this review I have tried to summarize some of the main aspects of nuclear shell structure and highlighted some of the main drivers of shell modifications far away from stability. Quite dramatic changes of shell structure occur in the neutron-rich region of the nuclear chart, in particular in light nuclei, as indicated in figure 9. For example, the $N=20$ and 28 shell closures break down and new magic numbers appear at $N=16$ for $Z=6,8$ and $N=34$ for $Z=20$. The discovery of such major changes to the magic numbers, which were previously thought to be valid throughout the whole nuclear chart, has led to vigorous experimental and theoretical activities to understand the origin of these changes and to make predictions for those nuclei not accessible to experimental studies yet. From the above discussion of nuclei near ^{132}Sn one realizes that the effect of the monopole interaction and any changes of the spin-orbit interaction can contribute to the observed changes of the single-particle structure at the same time and need to be carefully disentangled. In addition, other effects can come into play, such as changes of the nuclear pairing correlations, collective correlations, or the coupling of bound states to unbound continuum states.

The complexity of these issues is one reason why it is essential to obtain multiple and detailed experimental observables on the single-particle structure far away from stability. The development of facilities for exotic nuclear beams have been an essential driver for these studies. However, due to the difficulties in producing the nuclei of interest and the low intensities of those exotic nuclear beams, the experiments are very challenging and need ingenious technological and methodological developments to succeed. It is this combination of theoretical and experimental challenges, which make the field of nuclear structure of exotic nuclei so interesting.

The radioactive beam facilities of the next generation like RIBF at RIKEN (Japan), FAIR at GSI Darmstadt (Germany), and FRIB at MSU (U.S.A.) as well as HIE-ISOLDE at CERN, SPIRAL2 at GANIL (France) and possibly EURISOL will provide access to even more exotic nuclei, in particular along the r-process path and all the way towards the neutron dripline for medium-mass nuclei. With these facilities and the immense theoretical efforts to develop a unified theoretical framework for the description of the structure and dynamics of nuclei the evolution of shell structure in atomic nuclei will be possible to develop a coherent understanding of the nuclear many body system and link it to the other facets of the phases and structures of strongly interacting matter.

Acknowledgements

I would like to thank J. Friese, R. Gernhäuser, and D. Mücher for the careful reading of this manuscript and many thought provoking discussions.

References

- [1] P.F. Bedaque, U. van Kolck, *Ann. Rev. Nucl. Part. Sci.* 52, 339 (2002).
- [2] E. Epelbaum, *Prog. Part. Nucl. Phys.* 57, 654 (2006).
- [3] P. Finelli, N. Kaiser, D. Vretenar, W. Weise, *Nucl. Phys. A* 770, 1 (2006).
- [4] E. Epelbaum, H.-W. Hammer, U.-G. Meißner, *Rev. Mod. Phys.* 81, 1773 (2009).
- [5] L. Coraggio, A. Covello, A. Gargano, N. Itaco, T.T.S. Kuo, *Prog. Part. Nucl. Phys.* 62, 135 (2009).
- [6] P.J. Wood, C.N. Davids, *Ann. Rev. Nucl. Part. Sci.* 47, 541 (1997).
- [7] P.G. Hansen and J. A. Tostevin, *Annu. Rev. Nucl. Part. Sci.* 53, 219 (2003).
- [8] T. Aumann, *Eur. Phys. J. A* 26, 441 (2005).
- [9] N. Keeley, R. Raabe, N. Alamanos, J.L. Sida, *Prog. Part. Nucl. Phys.* 59, 579 (2007).
- [10] N. Paar, D. Vretenar, E. Khan, G. Colo, *Rep. Prog. Phys.* 70, 691 (2007).
- [11] M.A. Bentley, S.M. Lenzi, *Prog. Part. Nucl. Phys.* 59, 497 (2007).
- [12] B. Blank, M.J.G. Borge, *Prog. Part. Nucl. Phys.* 60, 403 (2008).
- [13] A. Gade, Th. Glasmacher, *Prog. Part. Nucl. Phys.* 60, 161 (2008).
- [14] N. Keeley, N. Alamanos, K.W. Kemper, K. Rusek, *Prog. Part. Nucl. Phys.* 63, 396 (2009).
- [15] W. Elsasser, *J. de Phys. et Rad.* 5, 625 (1934).
- [16] M. Goeppert-Mayer, *Phys. Rev.* 74, 235 (1948).
- [17] F. Käppeler, H. Beer, K. Wisshak, *Rep. Prog. Phys.* 52, 945 (1989).
- [18] H. Grawe, K. Langanke, G. Martinez-Pinedo, *Rep. Prog. Phys.* 70, 1525 (2007).
- [19] E.M. Burbidge, G. R. Burbidge, W. A. Fowler, and F. Hoyle, *Rev. Mod. Phys.* 29, 547 (1957).
- [20] B. Chen et al., *Phys. Lett. B* 355, 37 (1995).
- [21] B. Pfeiffer, K.-L. Kratz, F.-K. Thielemann, *Z. Phys. A* 357, 235 (1997).
- [22] B. Pfeiffer, et al., *Nuclear Phys. A* 693, 282 (2001).
- [23] J.J. Cowan, F.-K. Thielemann, J.W. Truran, *Phys. Rep.* 208, 267 (1991).
- [24] B.S. Meyer, G.J. Mathews, W.M. Howard, S.E. Woosley, R.D. Hoffman, *Astrophys. J.* 399, 656 (1992).
- [25] S.E. Woosley, R.D. Hoffmann, *Astrophys. J.* 395, 202 (1992).
- [26] I.V. Panov, H.-Th. Janka, *Astronomy & Astrophysics* 494, 829 (2009).
- [27] R. Surman, G.C. McLaughlin, M. Ruffert, H.-Th. Janka, W.R. Hix, *Astrophysical Journal Letters* 679, L117 (2008).
- [28] P. Ring, P. Schuck, *The nuclear many-body problem*, Springer-Verlag, New York (1980), p.3.
- [29] M. Goeppert-Mayer, *Phys. Rev.* 75, 1969 (1949).
- [30] O. Haxel, J.H.D. Jensen, H.E. Suess, *Phys. Rev.* 75, 1766 (1949).
- [31] M. Bender, P.H. Heenen, P.G. Reinhard, *Rev. Mod. Phys.* 75, 121 (2003).
- [32] D. Vretenar, A.V. Afanasjev, G.A. Lalazissis, P. Ring, *Phys. Rep.* 409, 101 (2005).
- [33] S.C. Pieper and V. R. Pandharipande, *Phys. Rev. Lett.* 70, 2541 (1993).
- [34] T. Otsuka, T. Suzuki, M. Honma, Y. Utsuno, N. Tsunoda, K. Tsukiyama, M. Hjorth-Jensen, arXiv:0908.2607 [nucl-th].
- [35] B.H. Wildenthal, *Prog. Part. Nucl. Phys.* 11, 5 (1984).
- [36] K.A. Brueckner, *Phys. Rev.* 97, 1353 (1955).
- [37] J. Goldstone, *Proc. Roy. Soc. A* 293, 267 (1957).
- [38] M. Hjorth-Jensen, T.T.S. Kuo, E. Osnes, *Physics Reports* 261, 125 (1995).
- [39] B.A. Brown, *Prog. Part. Nucl. Phys.* 47, 517 (2001).
- [40] D.J. Dean, T. Engeland, M. Hjorth-Jensen, M.P. Kartamyshev, E. Osnes, *Prog. Part. Nucl. Phys.* 53, 419 (2004).
- [41] E. Caurier, G. Martinez-Pinedo, F. Nowacki, A. Poves, A.P. Zuker, *Rev. Mod. Phys.* 77, 427 (2005).
- [42] S. Bogner, T.T.S. Kuo, L. Coraggio, *Nucl. Phys. A* 684, 432c (2001).
- [43] S. Bogner, et al., *Phys. Rev. C* 65, 051301(R) (2002).
- [44] S. Bogner, T.T.S. Kuo, A. Schwenk, *Phys. Rep.* 386, 1 (2003).
- [45] K. Heyde, J. Jolie, J. Moreau, J. Ryckebusch, M. Waroquier, P. Van Duppen and, M. Huyse, J. L. Wood, *Nucl. Phys.* A466, 189 (1987).
- [46] A. Poves, A. Zuker, *Phys. Rep.* 70, 235 (1981).
- [47] Y. Utsuno, T. Otsuka, T. Mizusaki, M. Honma, *Phys. Rev. C* 60, 054315 (1999).
- [48] T. Otsuka, R. Fujimoto, Y. Utsuno, B.A. Brown, M. Honma, T. Mizusaki, *Phys. Rev. Lett.* 87, 082502 (2001).
- [49] T. Otsuka, T. Suzuki, R. Fujimoto, H. Grawe, Y. Akaishi, *Phys. Rev. Lett.* 95, 232502 (2005).
- [50] T. Otsuka, T. Matsuo, D. Abe, *Phys. Rev. Lett.* 97, 162501 (2006).
- [51] T. Otsuka et al., *Phys. Rev. Lett.* 104, 012501 (2010).
- [52] K. Blaum, *Physics Reports* 425, 1 (2006).
- [53] K. Blaum, *Contemp. Phys.* 51, 149 (2010).
- [54] B. Franzke, *Nucl. Instr. and Meth. B* 24/25 (1987) 18.
- [55] B. Franzke, H. Geissel, G. Münzenberg, *Mass Spectr. Reviews* 27, 428 (2008).
- [56] M. Hausmann et al., *Nucl. Instr. Meth. A* 446, 569 (2000).
- [57] T. Radon et al., *Nucl. Phys. A* 677, 75 (2000).
- [58] G. Audi, A.H. Wapstra and C. Thibault, *Nucl. Phys. A* 729, 337 (2003).
- [59] K. Alder, A. Bohr, T. Huus, B. Mottelson, A. Winther, *Rev. Modern Phys.* 28, 432 (1956).
- [60] K. Alder, A. Winther, *Coulomb Excitation*, Academic Press, New York, 1966.
- [61] J.A. Brown et al., *Phys. Rev. Lett.* 66, 2452 (1991).
- [62] M. Oshima et al., *Nucl. Instr. Meth. A* 312, 425 (1992).
- [63] O. Niedermaier et al., *Phys. Rev. Lett.* 94, 172501 (2005).
- [64] T. Motobayashi et al., *Phys. Lett. B* 346, 9 (1995).

- [65] T. Glasmacher, *Annu. Rev. Nucl. Part. Sci.* 48, 1 (1998).
- [66] F. Tondeur, *Z. Phys. A* 288, 97 (1978)
- [67] P. Haensel and J. L. Zdunik, *Astron. Astrophys.* 222, 353 (1989).
- [68] J. Dobaczewski, I. Hamamoto, W. Nazarewicz, and J. A. Sheikh, *Phys. Rev. Lett.* 72, 981 (1994).
- [69] J.M. Pearson, R. C. Nayak, and S. Goriely, *Phys. Lett. B* 387, 455 (1996).
- [70] G.A. Lalazissis, D. Vretenar, W. Pöschl, and P. Ring, *Phys. Lett. B* 418, 7 (1998).
- [71] O. Sorlin, M.-G. Porquet, *Prog. Part. Nucl. Phys.* 61, 602 (2008).
- [72] A. Ozawa, T. Kobayashi, T. Suzuki, K. Yoshida, I. Tanihata, *Phys. Rev. Lett.* 84, 5493 (2000).
- [73] C.R. Hoffman, et al. *Phys. Lett. B* 672, 17 (2009).
- [74] R. Kanungo et al., *Phys. Rev. Lett.* 102, 152501 (2009).
- [75] H. Geissel et al., *Nucl. Instr. Meth. B* 70, 286 (1992).
- [76] R.V.F. Janssens, *Nature* 459, 1069 (2009).
- [77] E. K. Warburton, J. A. Becker, and B. A. Brown, *Phys. Rev. C* 41, 1147 (1990).
- [78] W. Schwerdtfeger et al., *Phys. Rev. Lett.* 103, 012501 (2009).
- [79] P. Doornenbal et al., *Phys. Rev. Lett.* 103, 032501 (2009).
- [80] R. Kanungo et al., *Phys. Lett. B* 685, 253 (2010).
- [81] M. Honma, T. Otsuka, B.A. Brown, T. Mizusaki, *Phys. Rev. C* 65, 061301(R) (2002).
- [82] A. Poves et al., *Nucl. Phys. A* 694, 157 (2001).
- [83] E. Caurier et al., *Eur. Phys. J. A* 15, 145 (2002).
- [84] A. Poves, F. Nowacki, E. Caurier, *Phys. Rev. C* 72, 047302 (2005).
- [85] P. Maierbeck et al., *Phys. Lett. B* 675, 22 (2009).
- [86] I. Dillmann, et al., *Phys. Rev. Lett.* 91, 162503 (2003).
- [87] A. Jungclaus, et al., *Phys. Rev. Lett.* 99, 132501 (2007).
- [88] J.P. Schiffer, et al., *Phys. Rev. Lett.* 92, 162501 (2004).
- [89] P.T. Hosmer et al., *Phys. Rev. Lett.* 94, 112501 (2005).
- [90] J. Van de Walle et al., *Phys. Rev. Lett.* 99, 142501 (2007).
- [91] S. Baruah et al., *Phys. Rev. Lett.* 101, 262501 (2008).
- [92] J. Hakala et al., *Phys. Rev. Lett.* 101, 052502 (2008).
- [93] S.J. Steer et al., *Phys. Rev. C* 78, 061302 (2008).
- [94] N. Al-Dahan et al., *Phys. Rev. C* 80, 061302 (2009).
- [95] Z. Podolyak et al., *Phys. Lett. B* 672, 116 (2009).
- [96] B. Blank et al., *Phys. Rev. Lett.* 84, 1116 (2000).
- [97] C. Dossat et al., *Phys. Rev. C* 72, 054315 (2005).
- [98] D. Bazin et al., *Phys. Rev. Lett.* 101, 252501 (2008)
- [99] T. Faestermann et al., contribution to the 5th Int. Conf. on Exotic Nuclei and Atomic Masses (ENAM'08), Septmebter 7-13, 2008, Ryn, Poland.
- [100] Ch. Hinke, Dissertation, TU München, 2010.
- [101] K. Eppinger, Dissertation, TU München, 2010.
- [102] A. Sobiczewski, K. Pomorski, *Prog. Part. Nucl. Phys.* 58, 292 (2007).
- [103] S. Hofmann, G. Münzenberg, *Rev. Mod. Phys.* 72, 733 (2000).
- [104] Yu. Oganessian, *J. Phys. G* 34, R165 (2007).